5th Joint International Symposium on Deformation Monitoring (JISDM), 20-22 June 2022, Valencia, Spain
DOI: http://doi.org/10.4995/JISDM2022.2022.13885

Monitoring instabilities by MT-InSAR in a mesa placed town (Arjona, Guadalquivir valley, South Spain)

Antonio Miguel Ruiz-Armenteros[1, 2, 3], Mario Sánchez-Gómez[2, 4], José Manuel Delgado-Blasco[3], Matus Bakon[5, 6], Ana Ruiz-Constán[7], Jesús Galindo-Zaldívar[8, 9], Milan Lazecky[10, 11], Miguel Marchamalo-Sacristán[12], Joaquim J. Sousa[13, 14]

[1] Department of Cartographic, Geodetic and Photogrammetry Engineering, University of Jaén, Campus Las Lagunillas s/n, 23071 Jaén, Spain, (amruiz@ujaen.es)
[2] Centre for Advanced Studies in Earth Sciences, Energy and Environment (CEACTEMA), University of Jaén, Campus Las Lagunillas s/n, 23071 Jaén, Spain
[3] Research Group RNM-282 Microgeodesia Jaén, University of Jaén, Campus Las Lagunillas s/n, 23071 Jaén, Spain, (jdblasco@ujaen.es)
[4] Department of Geology, University of Jaén, Campus Las Lagunillas s/n, 23071 Jaén, Spain, (msgomez@ugr.es)
[5] insar.sk s.r.o., Slovakia, (matusbakon@insar.sk)
[6] Department of Finance, Accounting and Mathematical Methods, University of Presov, Slovakia
[7] Instituto Geológico y Minero de España, 18006 Granada, Spain, (a.ruiz@igme.es)
[8] Department of Geodynamics, University of Granada, 18071 Granada, Spain, (jgalindo@ugr.es)
[9] Instituto Andaluz de Ciencias de la Tierra (CSIC-UGR), Granada, Spain
[10] School of Earth and Environment, University of Leeds, United Kingdom, (M.Lazecky@leeds.ac.uk)
[11] IT4Innovations, VSB-TU Ostrava, Czechia
[12] Topography and Geomatics Lab. ETS ICCP, Universidad Politécnica de Madrid, 28040 Madrid, Spain, (miguel.marchamalo@upm.es)
[13] Universidade de Trás-os-Montes e Alto Douro, Vila Real, Portugal, (jjsousa@utad.pt)
[14] INESC-TEC - INESC Technology and Science, Porto, 4200-465, Portugal

Key words: *InSAR; landslide; deformation; monitoring; mesa; satellite radar interferometry*

ABSTRACT

Cities in Spain used to be overgrown around old towns (pre-roman, roman and medieval) constructed on topographic defensive heights of singular geological features. In the upper Guadalquivir valley, a tabular body of Miocene sediments has been eroded forming mesas where most of its population has been living since the Middle Age. As the towns grew, new neighborhoods settled towards the edges and cliffs of these mesas, in areas prone to instability. The town of Arjona is a good example of this geological-urbanistic setup, located on the tabular hill formed by clay marls topped by bioclastic limestones that protect it from erosion. Modern buildings from a few sectors of the town show important cracks, even the 16th-century bell tower has a 4° inclination indicating problems in the foundations. Multi-temporal SAR interferometry (MT-InSAR) is a powerful technique to derive displacement time series over coherent targets on the Earth associated with geological or structural instabilities phenomena. In this work, we use MT-InSAR with Sentinel-1 data to reveal that, at the present day, the periphery of Arjona is active, being recognized a large landslide in the south side of this mesa town which affects buildings and civil infrastructures. In addition, fieldwork is being carried out to investigate the sources of these instabilities.

I. INTRODUCTION

Small cities and towns in Spain used to be integrated into a rural environment, where slope instabilities are common due to relief evolution and land management. Southern Spain is a geologically active area with an important tectonic uplift since the Pliocene (Sanz de Galdeano and Alfaro, 2004). Thus, high gradients together with soft lithologies produce slope instabilities even in areas of arid and semi-arid climate.

Cities in Spain used to be overgrown around old towns (pre-roman, roman and medieval) constructed on topographic defensive heights (Ruiz and Molinos, 1993; Castillo-Armenteros, 1998). As the towns grew, new neighborhoods settled towards the edges and cliffs, in areas with high probabilities of instability. The town of Arjona, in the Upper Guadalquivir valley, is a good example of this topographic-urbanistic setup and is subject to slope movements due to its singular topographic and geological features.

BY-NC-SA 2022, Editorial Universitat Politècnica de València

Most of the slope movements in the region are related to highly rainy events that show a return period greater than 10-20 years (Carpena *et al.*, 2021). In these events, landslides can be exhaustively followed by photogrammetry and LiDAR techniques (Fernández *et al.*, 2021), or by UAV surveys (Fernández *et al.*, 2016). Nevertheless, slow and continuous displacements must be previously identified by a technique that covers a much larger area such as the Interferometric Synthetic Aperture Radar (InSAR) technique. In this sense, the study of the highly settled towns in the Upper Guadalquivir by InSAR could provide valuable information about natural slope processes that modern urbanization has masked out and that suppose an important hazard.

Interferometric Synthetic Aperture Radar (InSAR) technique can provide more detailed land deformation mapping over larger areas than any other technique. InSAR is successfully applied for monitoring natural hazards such as volcanoes, landslides, and earthquakes/tremors. The advantages of this technique are its cost-effectiveness and very precise measurement of land deformation, and in the areas with good radar scattering characteristics, it is theoretically possible to detect even millimeter-sized surface deformation. Measurements can be done entirely retroactively by acquiring historic repeat satellite Synthetic Aperture Radar (SAR) datasets for the area of interest, and then processing the SAR data using interferometric techniques to determine changes in the distance satellite-terrain over large areas with high precision. The technique allows us to have a global outlook of the deformation phenomena occurring in a wider area, keeping at the same time the capability to measure deformation at millimeter accuracy on individual features, like dams, bridges, or buildings using multi-temporal interferometric techniques (MT-InSAR) (Crosetto *et al.*, 2016; Xue *et al.*, 2020; Ho Tong Minh *et al.*, 2020).

This paper presents the preliminary results from the application of MT-InSAR techniques to land deformation monitoring in the study of mesa towns. In particular, some deformation spots are identified in Arjona town and its temporal evolution is studied using Sentinel-1 SAR data, which is related to the geological/geomorphological processes that configure the relief. A field survey will corroborate the nature of the displacements.

II. Geographical and Geological settings

The Arjona town is located in the Upper Guadalquivir valley (Figure 1) that coincides approximately with the administrative province of Jaén (south Spain). The Upper Guadalquivir includes the headwater areas from Cazorla and Segura Ranges belonging to the Betic Cordillera. Discarding these Betic mountains, the valley varies in altitude from about 200 to 1000 m, with slopes generally below 10°.

Figure 1. Location of Arjona town in the province of Jaén (South Spain). Lat: 37.93652°, Lon: -4.0601° (Source: Google Maps).

The Guadalquivir valley is developed over the Betic foreland basin, which was an NE-SW elongated marine basin from the Lower Miocene until the Pliocene (García-Castellanos *et al.*, 2002). The Guadalquivir basin shows two contrasting margins. Towards the south, tectonic units from the Betic Thrust Front formed an accretionary prism imbricating sediments of the basin (Pérez-Valera *et al.*, 2017). Towards the north, Mesozoic and Miocene sediments of the basin above the Variscan basement form a near-horizontal cover, the so-called Tabular Cover, slightly folded and faulted (Pedrera *et al.*, 2013). Most of the deformation occurred during the Miocene (Pérez-Valera *et al.*, 2017), after which vertical isostatic readjustment caused regional uplift (Sanz de Galdeano and Alfaro, 2004). Nevertheless, there are evidences of Pleistocene and Holocene horizontal and vertical tectonic displacements (Sánchez-Gómez and Pérez-Valera, 2018), including an intense seismic activity (Pedrera *et al.*, 2013; Sánchez-Gómez *et al.*, 2014; Morales *et al.*, 2015).

The Miocene sedimentation consists in a sequence of alternances of sandstones and marls with large volumes of active clays, and relatively resistant layers of calcarenites (Martínez del Olmo and Martín-Sánchez, 2019). When the uplift of the basin after Pliocene exposed the sediments to erosion, the calcarenite, or thick sandstone, strata formed mesas along the Guadalquivir valley. These mesas are up to 400 m higher than the present Guadalquivir talweg, although abrupt slopes are only a few tens of meters high (Figure 2 top). The town of Arjona occupies one of these mesas of approximately 75 ha, with cliffs or steep slopes on the north and southeast sides, and a less defined border towards the west (Figure 2 bottom).

The Miocene marls below the resistant layers include a more than 140 m thick sequence of the so-called Blue Marls, a clay-rich formation with associated geotechnical problems on all the upper Guadalquivir valley. The Blue Marls in the region have an average of clay between 28% and 59%, and activity between 0.55

2022, Editorial Universitat Politècnica de València BY-NC-SA

and 0.88 (Mellado *et al.*, 2021). Geotechnically, these can be classified as inorganic clays of high plasticity (CH). This geotechnical context produced historical ground instabilities, as can be deduced from the 16thcentury bell tower with a 4º deviation from the vertical.

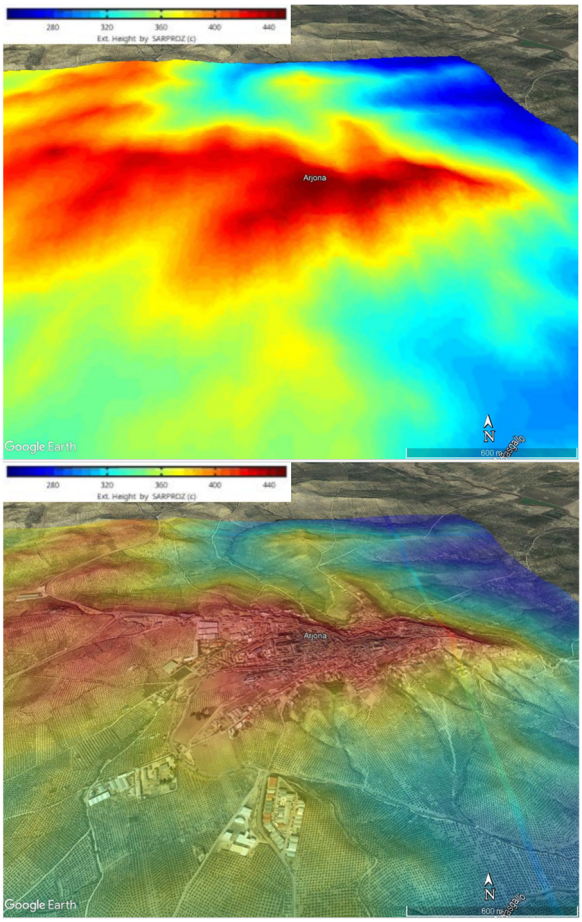

Figure 2. Top. 3D view of the 1-arcsec SRTM DEM over the study area. Heights range between 250 and 450 m. Bottom. 3D view of Arjona and the SRTM DEM. Arjona is located on the mesa formed in the highest altitudes of this area. (Source: Google Maps).

III. Data and methods

A. *InSAR data*

We used Sentinel-1A/B SLC data in our study. The ascending stack is composed of 314 IW images from Track 74 in the period March 3, 2015 – February 23, 2021, with an average incidence angle of 43.8443°. The descending dataset is composed of 340 IW images from Track 81 in the period March 16, 2015, to October 4, 2021, with an average incidence angle of 39.3819°. In both cases, the ground sampling is in the order of 3.5 x 13.8 m. Figure 3 shows the information of the ascending and descending datasets.

B. *Multi-temporal InSAR*

For processing the Sentinel-1 ascending and descending datasets we used a Multi-temporal time series analysis (MT-InSAR) using SARPROZ software, following the classical PS-InSAR approach (Ferretti *et al.*, 2001; Kampes, 2006).

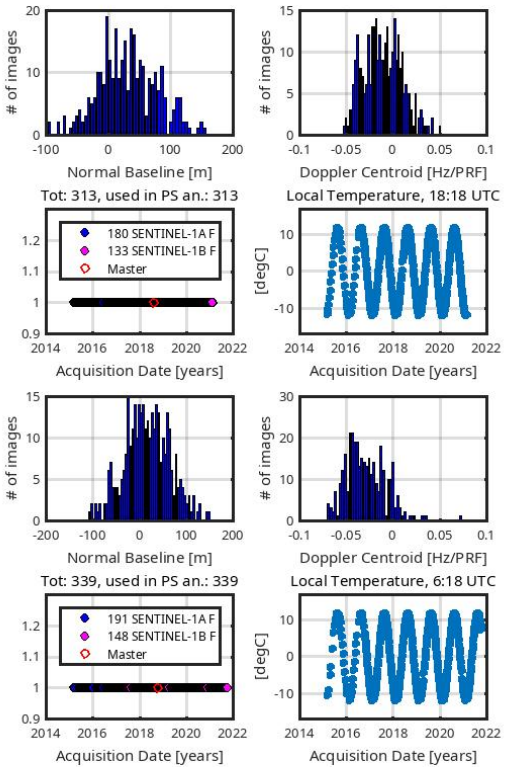

Figure 3. Information about the ascending (top) and descending (bottom) datasets. For both, the normal baseline and Doppler centroid plots are shown, together with the acquisition date and the synthetic temperature sinusoid for each acquisition time.

The objective of the PS-InSAR technique is to identify stable scatterers in a series of images and to separate the different phase components to isolate the phase displacement from the others, such as the atmospheric disturbance, topography, and flat-Earth terms. These stable scatterers, named Persistent Scatterers (PS), must remain physically stable along the period of study covered by the image stack, so they have high phase stability, and has to be smaller in size than the resolution cell, as they have a strong backscatter reflection of the incident wave to the satellite, avoiding the geometric decorrelation. The technique is particularly useful in urban environments because the man-made elements, such as buildings, road, railways, or exposed rocks, are not affected by geometrical and temporal decorrelation (Mazzanti *et al.*, 2015).

For each dataset, the first step is co-registering all the images with respect to a master image, selected by minimizing the temporal and perpendicular baselines in order to maximize the temporal coherence. The image acquired on August 2, 2018, was selected for the ascending dataset and on October 14, 2018, for the descending one (Figure 4).

After co-registering each dataset, the reflectivity map, that is, the temporal average of all the images in the stack, and the amplitude stability index (ASI) are computed. ASI is computed as 1-DA, where DA is the

BY-NC-SA 2022, Editorial Universitat Politècnica de València

amplitude dispersion index. DA is a measure of phase stability and is computed as the ratio between the standard deviation of a pixel and the mean amplitude value. If a pixel has a high amplitude, that is, small DA, similar in all the images, is expected to have minor phase dispersion than if it has low amplitude. Figure 5 shows the reflectivity maps for each dataset. It can be noted the low reflectivity of the terrain surrounding the town due to the fact that it is completely covered with olive tree plantings (Figure 1).

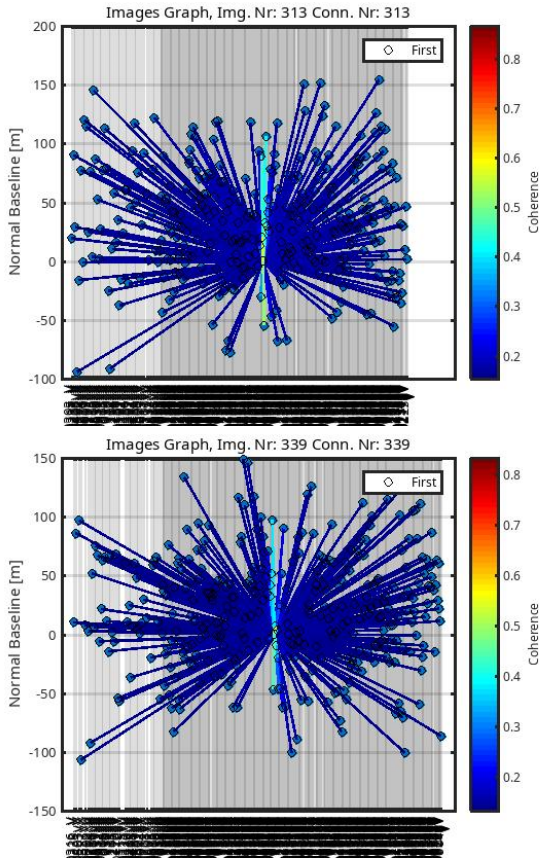

Figure 4. Normal vs. temporal baseline plots for the ascending (top) and descending (bottom) datasets. The ascending dataset is composed of 314 acquisitions from Track 74 in the period March 3, 2015 – February 23, 2021. The descending dataset is composed of 340 acquisitions from March 16, 2015, to October 4, 2021.

To remove the topographic phase component and geocode the results, we used the SRTM 1-arcsec DEM with 30 m resolution. After these initial steps, the Atmospheric Phase Screen (APS) is estimated based on the fact that the atmosphere is spatially but not temporally correlated, one of the main advantages of the MT-InSAR techniques. For this estimation, an initial spatial network is formed by an initial selection of PS candidates (PSC). The selection is done using the ASI index as phase stability with a threshold of 0.75. This network is used to estimate the DEM error (residual topographic phase term) and the deformation rate as the unknown parameters for each connection between two PSCs, maximizing a periodogram (Perissin *et al.*, 2012). To derive the deformation rates we assumed a linear model.

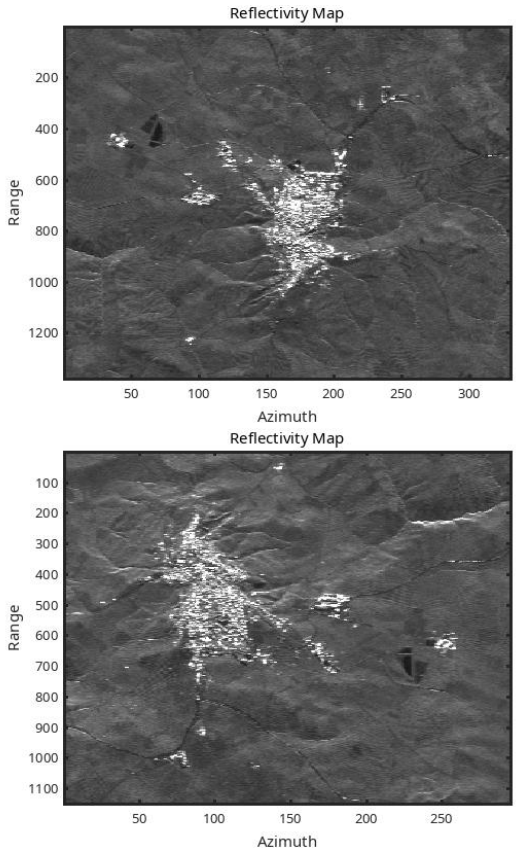

Figure 5. Reflectivity map for the ascending (top) and descending (bottom) datasets. They are shown in radar coordinates.

Phase differences are relative both in time and space, so, these deformation rates are computed with respect to a reference point supposedly stable and selected in this case in the center of the town. In the APS estimation, for the estimation of the atmospheric signal in the master image, the average residual phase is computed for each PSC after the correction for the modeled parameters. Using high-pass filtering, the atmospheric signal of each slave image and the phase noise are separated from the un-modeled deformation signal. To increase the density of PS, after the APS estimation, a second selection of PS is done based on a threshold, in this case, a lower value of ASI. Again, to re-estimate the unknown parameters, that is, the residual heights and velocity rates, another maximization of the periodogram is carried out. The final result is the height and the mean Line-of-Sight (LOS) velocity for each PS. The final selection of PS is filtered out based on the temporal coherence, which is a function of the residual phase noise.

IV. Result and Discussion

After the MT-InSAR analysis, the mean line-of-sight (LOS) velocity maps are derived for each dataset (Figure 6).

2022, Editorial Universitat Politècnica de València BY-NC-SA

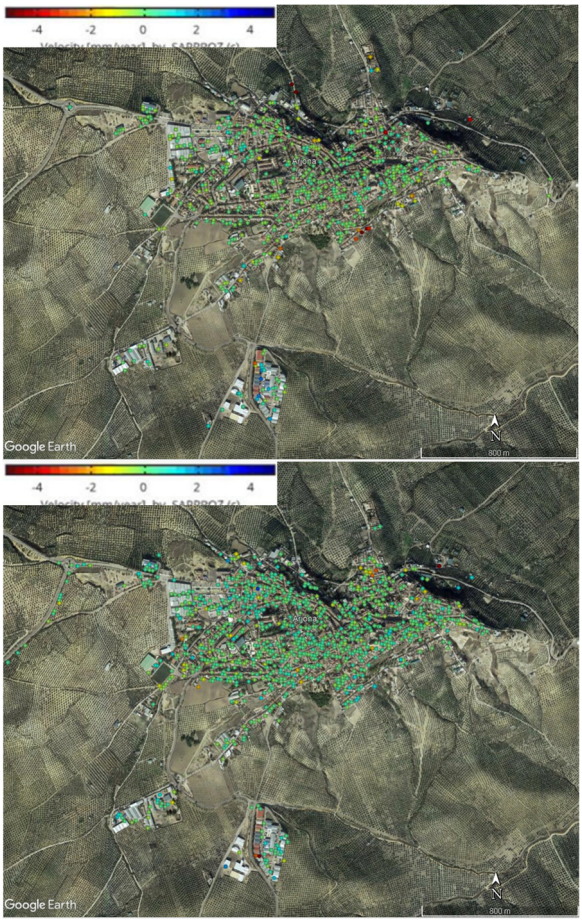

Figure 6. Mean LOS velocity map for the ascending (top) and descending (bottom) datasets.

Three sectors with a near-continuous movement have been identified: the southeast shoulder, the north foot-slope, and the northeast slope. Three time series plots are shown for these three areas respectively in Figure 7.

The movements of the southeast shoulder (Figure 7 top) can be interpreted as those of the crown of a large single mass movement. Almost all the houses of the street show cracks consistent with an incipient south-faced landslide (Figure 8), although the owners are not aware of this fact, and blame poor foundations.

The second sector, the north foot-slope (Figure 7 bottom), is situated in an area with limited inclination, and in the preliminary field survey, movements could be attributed to some kind of subsidence related to the operation of an irrigation well, located near to the observed targets. The causes of the northeast slope displacements (Figure 7 middle) are less clear, and it cannot be established a specific type of slope movement (*v.g.* creeping, local landslide). Nevertheless, the effects observed in the field are evident (Figure 9) and congruent with most of them.

All the described displacements have a velocity of very few mm/year. They occurred after 2015, a period particularly dry in the region. Recent studies (Carpena *et al.*, 2021) show that landslides and erosion in the Upper Guadalquivir are associated with recurrent wet periods that include rainfall events with a return period between 5 to 20 years. Thus, in the next foreseeable rainy event, it can be expected that the velocity of movement in the observed sectors will increase dramatically, producing even catastrophic episodes.

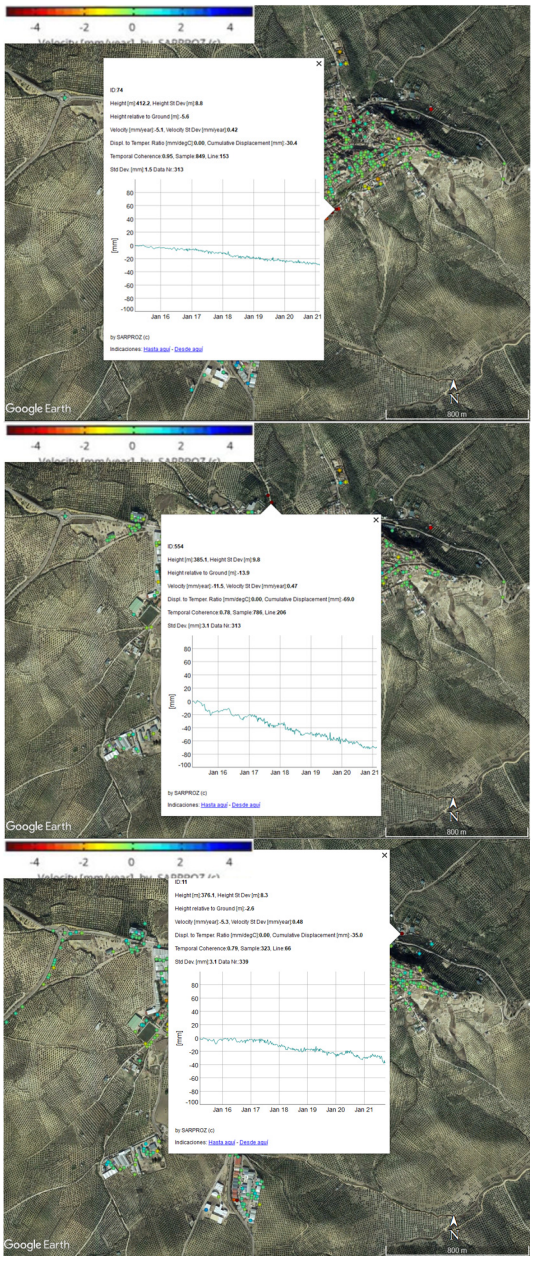

Figure 7. Time series plots of the LOS displacement for the three identified areas, the southeast shoulder (top), the northeast slope displacements (middle), and the north foot-slope (bottom).

V. Conclusions

MT-InSAR technique demonstrates the utility to detect silent slope processes. The good and stable reflectors found in the rural towns allow us to distinguish slow but continuous displacements and identify the geomorphological processes that originate them, particularly in historical villages grown above mesa hills. Vertical and horizontal movements are interpreted by the inhabitants as their own foundation problems, but they are unaware of the scope of the

BY-NC-SA 2022, Editorial Universitat Politècnica de València

processes in which they are involved. Then MT-InSAR should be considered a helpful tool for the risk assessment, and prevent catastrophic and recurrent episodes during rainfall events.

Figure 8. Cracks in a build from the southeast shoulder sector. The wall shown is oriented N160ºE (north to the left), the observed displacement being strictly parallel to this orientation.

Figure 9. Cracks in a build from the northeast slope sector. The shown wall is oriented N145ºE (northwest to the right). Other cracks can be seen in different walls of the same construction, not visible in the picture.

VI. Acknowledgements

Sentinel-1A/B data were freely provided by ESA through the Copernicus Programme. Data have been processed SARPROZ (Copyright (c) 2009-2022 Daniele Perissin). The satellite orbits are from ESA Quality control Group of Sentinel-1. Research was supported by: (a) Project "Identificación de riesgos geológicos en la provincia de Jaén mediante satélites de observación de la Tierra" from Instituto de Estudios Giennenses, Diputación Provincial de Jaén (2021-2022); (b) POAIUJA-2021/2022 and CEACTEMA from University of Jaén (Spain); (c) the convene "Risks associated to the Road Network of the Jaén Province" of the Jaén Provincial Council; and RNM-282 and RNM-325 research groups from the Junta de Andalucía (Spain). We thank M.M. Jiménez-Cañaveras for her assistance in the field work.

References

Carpena, R., Tovar-Pescador, J., Sánchez-Gómez, M., Calero, J., Mellado, I., Moya, F., and Fernández, T., (2021). Rainfall-induced landslides and erosion processes in the road network of the Jaén Province (Southern Spain). *Hydrology* 8, 100. DOI: 10.3390/hydrology8030100

Castillo-Armenteros, J.C., (1998). *La Campiña de Jaén en época emiral, siglo VIII-X*. Universidad de Jaén, 326 pp.

Crosetto, M., Monserrat, O., Cuevas-González, M., Devanthéry, N., and Crippa, B., (2016). Persistent scatterer interferometry: A review. *ISPRS Journal of Photogrammetry and Remote Sensing*, 115, pp. 78–89. DOI: 10.1016/j.isprsjprs.2015.10.011.

Fernández, T., Pérez, J.L., Cardenal, F.J., Gómez, J.M., Colomo, C., and Delgado. J., (2016). Analysis of Landslide Evolution Affecting Olive Groves Using UAV and Photogrammetric Techniques. *Remote Sensing* 8, 10: 837. DOI: 10.3390/rs8100837

Fernández, T., Pérez-García, J.L., Gómez-López, J.M., Cardenal, F.J., Moya, F., and Delgado, J., (2021). Multitemporal Landslide Inventory and Activity Analysis by Means of Aerial Photogrammetry and LiDAR Techniques in an Area of Southern Spai. *Remote Sensing* 13, 11: 2110. DOI: 10.3390/rs13112110

Ferretti, A., Prati, C., and Rocca, F., (2001). Permanent Scatterers in SAR interferometry. *IEEE Trans. Geosci. Remote Sens*., 39, 8–20.

García-Castellanos, D., Fernández, M., and Torné, M., (2002). Modeling the evolution of the Guadalquivir foreland basin (southern Spain). *Tectonics*, 21, 1018.

Ho Tong Minh, D., Hanssen, R., and Rocca, F., (2020). Radar Interferometry: 20 Years of Development in Time Series Techniques and Future Perspectives. *Remote Sensing*, 12; 1364.

Kampes, B.M., (2006). Radar Interferometry; Springer: Dordrecht, *The Netherlands*.

Martínez del Olmo, W., and Martín Sánchez, D., (2019). Surcos erosivos, sistemas de turbiditas y episodios climáticos en el Tortoniense y Messiniense de la Cuenca del Guadalquivir (SO de España). *Rev. la Soc. Geológica España* 32, pp. 97–112.

Mazzanti, P., Perissin, D., and Rocca, A., (2015). Structural health monitoring of dams by advanced satellite SAR interferometry: investigation of past processes and future monitoring perspectives. In 7th International Conference on Structural Health Monitoring of Intelligent Infrastructure, Torino, Italy.

Mellado, J.I., Calero, J.A., Sánchez-Gómez, M., Fernández, T., Carpena, R., and Pérez de la Torre, A., (2021).

2022, Editorial Universitat Politècnica de València BY-NC-SA

Caracterización litogeotécnica de las margas del Mioceno Superior del Alto Guadalquivir. In: Errandonea-Martín *et al.* (Eds.), *X Congreso Geológio de España*. Sociedad Geológica de España, Vitoria, p. 518.

Morales, J., Azañón, J.M., Stich, D., Roldán, F.J., Pérez-Peña, J.V., Martín, R., Cantavella, J.V., Martín, J.B., Mancilla, F., and González-Ramón, A., (2015). The 2012–2013 earthquake swarm in the eastern Guadalquivir basin (South Spain): A case of heterogeneous faulting due to oroclinal bending. *Gondwana Res.* 28, pp. 1566–1578. DOI: 10.1016/j.gr.2014.10.017

Pedrera, A., Ruiz-Constán, A., Marín-Lechado, C., Galindo-Zaldívar, J., González, A., and Peláez, J.A., (2013). Seismic transpressive basement faults and monocline development in a foreland basin (Eastern Guadalquivir, SE Spain). *Tectonics* 32, 2013TC003397. DOI: 10.1002/2013TC003397

Pérez-Valera, F., Sánchez-Gómez, M., Pérez-López, A., and Pérez-Valera, L.A., (2017). An evaporite-bearing accretionary complex in the northern front of the Betic-Rif Orogen. *Tectonics* 36, pp. 1006–1036. DOI: 10.1002/2016TC004414

Perissin, D., Wang, Z., and Lin, H., (2012). Shanghai subway tunnels and highways monitoring through Cosmo-SkyMed Persistent Scatterers. *ISPRS J. Photogramm. Remote Sens.* 2012, 73, pp. 58–67.

Ruiz, A., and Molinos, M., (1993). *Los Iberos. Análisis arqueológico de un proceso histórico*. Crítica, Barcelona. 325 pp.

Sánchez-Gómez, M., and Pérez-Valera, F., (2018). Evidence of recent tectonics (Late Pleistocene) at the Betic Cordillera-Guadalquivir Basin boundary (province of Jaén). In: Canora, C., Martín, F., Masana, E., Pérez, R., Ortuño, M. (Eds.), *III Reunión Ibérica Sobre Fallas Activas y Paleosismología*. Alicante (Spain), pp. 107–110.

Sánchez-Gómez, M., Peláez, J.A., García-Tortosa, F.J., Pérez-Valera, F., and Sanz de Galdeano, C., (2014). La serie sísmica de Torreperogil (Jaén, Cuenca del Guadalquivir oriental): evidencias de deformación tectónica en el área epicentral. *Rev. la Soc. Geol. España* 27, pp. 301–318.

Sanz de Galdeano, C., and Alfaro, P., (2004). Tectonic significance of the present relief of the Betic Cordillera. *Geomorphology* 63, pp. 175–190. DOI: 10.1016/j.geomorph.2004.04.002

Xue, F., LV, X., Dou, F., and Yun, Y., (2020). A Review of Time-Series Interferometric SAR Techniques. A tutorial for surface deformation analysis. *IEEE Geoscience and Remote Sensing Magazine*. March 2020.

BY-NC-SA 2022, Editorial Universitat Politècnica de València